

ARTICLE OPEN



Enhanced impact of the Aleutian Low on increasing the Central Pacific ENSO in recent decades

Shangfeng Chen¹, Wen Chen^{1,2}, Bin Yu³, Renguang Wu⁴, Hans-F. Graf⁵ and Lin Chen⁶

In this study, we reveal a marked enhanced impact of the early-spring Aleutian Low (AL) on the following winter El Niño and Southern Oscillation (ENSO) after the late-1990s. This enhanced impact of the early-spring AL may have an important contribution to the increased emergence of the central Pacific ENSO during recent decades. After the late-1990s, decrease (increase) in the early-spring AL strength tends to induce an anomalous cyclone (anticyclone) over subtropical North Pacific via wave-mean flow interaction. The associated westerly (easterly) wind anomalies to the south side of the subtropical anomalous cyclone (anticyclone) over the tropical western Pacific contribute to occurrence of central Pacific-like El Niño (La Niña) in the following winter via tropical Bjerknes feedback. Further, the subtropical anomalous cyclone (anticyclone) leads to sea surface temperature (SST) increase (decrease) in the equatorial Pacific in the following summer via wind-evaporation-SST (WES) feedback, which further contributes to succeeding central Pacific-like El Niño (La Niña). Enhanced impact of early-spring AL on ENSO is attributable to enhancement of the mean circulation over the North Pacific, which leads to increased wave-mean flow interaction and strengthened WES feedback after the late-1990s. The results offer the potential to advance our understanding of the factors for the reduced prediction skill of ENSO since the late-1990s.

npj Climate and Atmospheric Science (2023)6:29; <https://doi.org/10.1038/s41612-023-00350-1>

INTRODUCTION

The El Niño and Southern Oscillation (ENSO) is the dominant mode of the tropical air-sea coupling system^{1–4}, featured by large sea surface temperature (SST) anomalies in the tropical central and eastern Pacific, and accompanied by notable changes in the tropical atmospheric circulation and convection. ENSO has tremendous impacts on the climate, agriculture, ecosystems, water resource and the livelihoods of people worldwide^{5–10}. Therefore, identifying the factors leading to the occurrence of ENSO events and improving the prediction skill of ENSO are of critical importance.

The prediction skill of ENSO is found to decrease obviously since the late-1990s^{11,12}, corresponding to the time when the central Pacific (CP) type of El Niño has become more frequent^{13–15}. Extratropical atmospheric forcings over the North Pacific, particularly the North Pacific Oscillation (NPO, the second Empirical Orthogonal Function [EOF] mode of sea level pressure anomalies [SLP] over the North Pacific)¹⁶, are suggested to contribute significantly to the occurrence of the CP ENSO via the seasonal footprinting mechanism and trade wind charging mechanism^{17–25}. However, two recent studies indicated that the impact of the winter NPO on the following winter ENSO weakens largely after the late-1990s^{26,27}, suggesting that extratropical atmospheric variability related to the winter NPO cannot totally explain the recent increased emergence of the CP ENSO.

Then, what might be other sources of atmospheric variability over the North Pacific that contributed to the recent frequent occurrence of CP ENSO events? This study finds that the early-spring (March) Aleutian Low (AL) may play an important role though prevailing view generally suggested a marked impact of the ENSO on the AL rather than the opposite effect^{6,28,29}. The AL

intensity variation represents the first leading mode of atmospheric variability over the North Pacific and explains more variance than the NPO¹⁸ (Supplementary Fig. 1). A recent study has preliminarily recognized that variation in the early-spring AL intensity has a marked impact on the following winter ENSO according to multiple reanalysis and observational data over 1979–2016³⁰. However, whether the recent increased occurrence of CP ENSO after the late-1990s is related to the impact of the early-spring AL remains unclear. In this study, we demonstrate that the impact of the early-spring AL on the following winter ENSO shows a marked enhancement after the late-1990s. We suggest that this enhanced impact of the early-spring AL may play an important role in the increased occurrence of the CP type ENSO events during recent decades. The physical mechanism for the enhanced impact of the early-spring AL is also examined. Results of this study may further improve our understanding of the change in the ENSO type and improve the understanding of the process for the impact of mid-high latitude atmospheric variability on ENSO type.

RESULTS

Strengthened impact of the March AL on ENSO

The connection of the March AL intensity index (ALI, defined as region-mean SLP anomalies over 30°–65°N and 160°E–140°W) with the following winter ENSO shows a stepwise increase during 1948–2020 (Fig. 1a, note that hereafter ENSO signal in preceding winter has been removed from the March ALI to avoid the impact of the ENSO cycle, please see “Methods”). The significant relationship of the March ALI with the following winter Niño-3.4 SST index can only be observed after the late-1990s (Fig. 1a), in

¹Center for Monsoon System Research, Institute of Atmospheric Physics, Chinese Academy of Sciences, Beijing, China. ²Department of Atmospheric Sciences, Yunnan University, 650500 Kunming, China. ³Climate Research Division, Environment and Climate Change Canada, Toronto, ON, Canada. ⁴School of Earth Sciences, Zhejiang University, Hangzhou, China. ⁵Center for Atmospheric Science, University of Cambridge, Cambridge, UK. ⁶Key Laboratory of Meteorological Disaster of Ministry of Education, Nanjing University of Information Science and Technology, Nanjing, China. ✉email: chenwen-dq@ynu.edu.cn

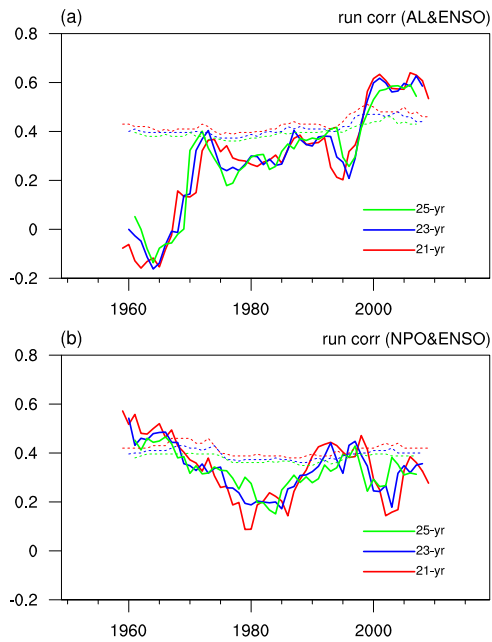


Fig. 1 Correlations of ENSO with preceding AL and NPO. Running correlation coefficients of **a** early-spring (Mar(0)) AL intensity (ALI) index and **b** winter (D(-1)JF(0)) NPO index with the following winter (D(0)JF(+1)) Niño-3.4 SST index with different moving lengths. Time notations “-1”, “0” and “+1” refer to the preceding, current and following years, respectively. Dashed lines indicate the corresponding running correlations significant at the 95% confidence level. Effective degree of freedom was considered when estimating significance level of correlation (see “Effective degree of freedom” in “Methods”). Years in **a**, **b** are labeled according to the central years of the running correlation.

line with the time that CP type ENSO events became more frequent^{13–15,18–20}. After the late-1990s, 7 out of 8 weakened AL years (“Methods”) are followed by El Niño events in the subsequent winter (Supplementary Table 1). The occurrences of the recent five CP El Niño events (i.e., 2002–03, 2004–05, 2006–07, 2009–10 and 2015–16, “Methods”) are all preceded by weakened spring AL years. In addition, 6 out of the 7 enhanced AL years are followed by La Niña events (Supplementary Table 1). This result suggests that the occurrence ratio of ENSO events is near 90% associated with the March AL after the late-1990s. Thus, the impact of the March AL on the tropical Pacific SST is suggested to be an important factor for the increased occurrence of the CP-type ENSO events since the late-1990s.

Studies generally suggested that the recent increased occurrence of the CP ENSO events was related to the winter NPO-related atmospheric forcing^{19,20}. The correlation of the winter NPO index (“Methods”) with the following winter Niño-3.4 SST index becomes weaker and insignificant after the late-1990s (Fig. 1b), consistent with recent studies^{26,27}. Particularly, the correlation between the winter NPO index and following winter Niño-3.4 SST index is only 0.34 (cannot past the 90% confidence level) after the late-1990s, about half of the correlation between the March ALI and the following winter Niño-3.4 SST index ($r = 0.63$). In addition, after the late-1990s, only 3 of 6 (4 of 7) positive (negative) winter NPO years are followed by El Niño (La Niña) events (Supplementary Table 1). The occurrence ratio of ENSO events is about 50% under condition of the winter NPO after the late-1990s, much lower than that of March ALI. Moreover, the three positive winter NPO years (i.e., 2005–06, 2010–11, and 2011–12) are even followed by La Niña events in the following winter. Above results suggest that the March AL may play a more important role for the

increased occurrence of the CP ENSO events after the late-1990s compared to the NPO.

Mechanisms for the strengthened impact of the AL on ENSO

It is necessary to understand the causes for occurrence of the recent enhanced impact of the March AL on the following winter ENSO. According to Fig. 1a, we separate the entire period into two sub-periods: 1949–1995 and 1996–2020. The difference in the correlation coefficient between periods 1996–2020 ($r = 0.63$) and 1949–1995 ($r = 0.12$) is significant at the 99% confidence level according to the Fisher’s r - z transformation (“Methods”).

We then examine evolutions of SST, 850-hPa winds and precipitation related to the March AL in the above two periods. After the late-1990s, the weakened AL in preceding spring is associated with a dipole atmospheric anomaly pattern over the North Pacific (Fig. 2a). Formation of the anomalous cyclone over the subtropical North Pacific is attributable to the interaction between mean flow and synoptic-scale eddy activity³⁰. Particularly, weakened AL in Mar(0) is associated with anomalous easterly winds (Fig. 2a) and EP flux convergence anomalies around 30°–40°N over the North Pacific (see extended EP flux in “Methods”) (Fig. 3a). These EP flux convergence anomalies are accompanied by pronounced positive geopotential height tendencies to the north and negative geopotential height tendencies to the south (Fig. 3b, see geopotential height tendencies in “Methods”), explaining formation of the cyclonic circulation anomaly over the subtropical North Pacific³⁰. Westerly wind anomalies to the south of the subtropical anomalous cyclone over the tropical western Pacific could lead to SST warming in the tropical central-eastern Pacific via zonal oceanic advection and triggering eastward propagating and downwelling Kelvin waves, which is confirmed by an analysis of the mixed layer heat budget (Supplementary Fig. 2, “Methods”). In addition, the subtropical cyclonic anomaly reduces the total wind speed and leads to ocean surface warming over subtropical northeastern Pacific in the late-spring via reduction of surface heat flux (Fig. 2g). SST anomaly pattern in Fig. 2g bears a resemblance to the Pacific meridional mode (PMM)^{31,32}. The late-spring ocean surface warming in the subtropical North Pacific extends southward to the equatorial central Pacific via wind-evaporation-SST feedback mechanism^{31,33,34}, which further develops to an El Niño event in the following winter via the Bjerknes-like positive air-sea interaction (Fig. 2b–e, g–j). Note that SST anomalies in the tropical Pacific and 850-hPa winds anomalies in the subtropical North Pacific are weak in preceding winter (Supplementary Fig. 3), suggesting that the impact of the March AL on the following winter ENSO is not due to the ENSO cycle.

Before the late-1990s, an atmospheric dipole anomaly pattern also appears over the North Pacific (Supplementary Fig. 4a). However, the subtropical anomalous cyclone is much weaker. Correspondingly, ocean surface warming is less obvious in the subtropical northeastern Pacific (Supplementary Fig. 4g) compared to that after the late-1990s (Fig. 2g). Therefore, March AL-related SST and atmospheric anomalies cannot extend to the tropical central Pacific, and thus have weak impacts on the following winter ENSO^{23,30} (Supplementary Fig. 4g–j).

The most important system in connecting the March AL to the following winter ENSO is the cyclonic anomaly over the subtropical North Pacific, and associated westerly wind anomalies to its south over the tropical western-central Pacific (TWCP). Figure 4a shows a scatter plot between the 23-year moving correlations of the March AL with the following winter ENSO against the corresponding AL-related westerly wind anomalies over the TWCP in AM(0). It shows that in decades when the March AL-related westerly wind anomalies over the TWCP are strong (weak), impact of the March AL on the following winter ENSO is strong (weak) (Fig. 4a).

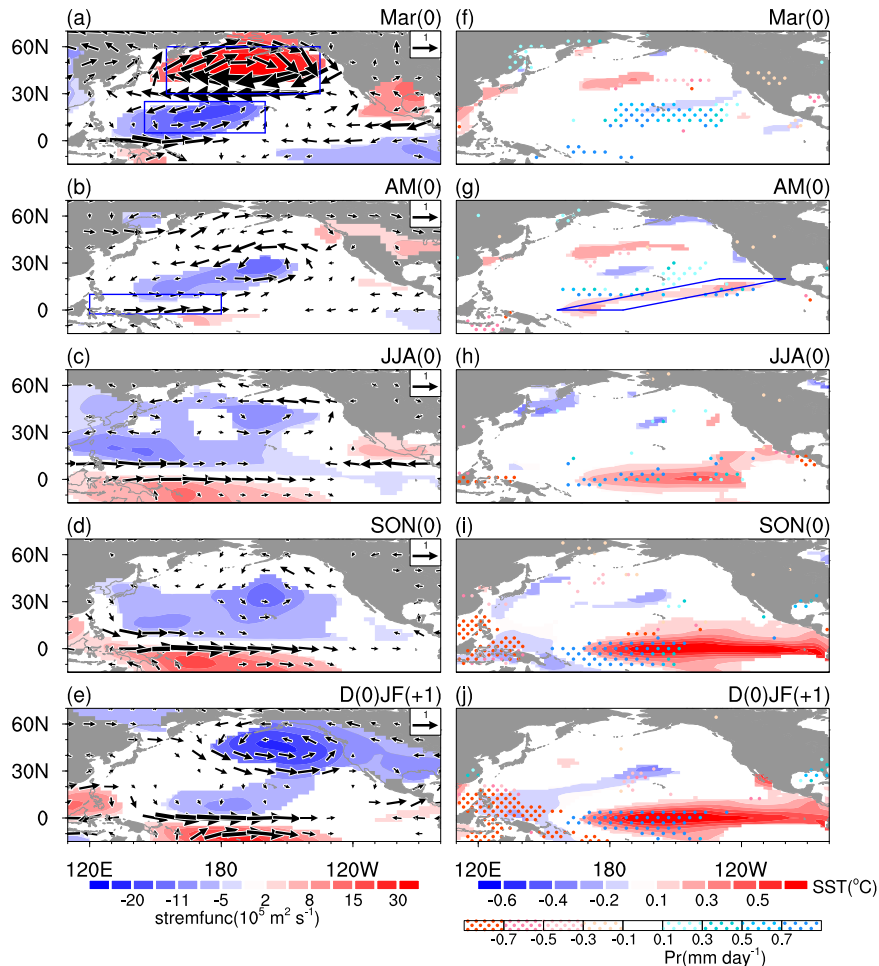


Fig. 2 Evolutions of SST and atmospheric anomalies related to the early spring ALI. Anomalies of 850-hPa stream function (shading) and winds (vector) in **a** Mar(0), **b** AM(0), **c** JJA(0), **d** SON(0), and **e** D(0)JF(+1) regressed upon the normalized ALI in Mar(0) over 1996–2018. **f–j** as in **a–e**, but for the evolutions of SST (shading) and precipitation (stippling) anomalies. Only the SST, precipitation and stream function anomalies exceeding the 95% confidence level are shown.

What are the plausible factors for the change of the March AL-related westerly wind anomalies over the TWCP? The amplitude of the March AL-related cyclonic anomaly over the subtropical western-central North Pacific after the late-1990s (Fig. 2a) is approximately two times stronger than that before the late-1990s (Supplementary Fig. 4a). The stronger cyclonic anomaly over the subtropical North Pacific can lead to stronger westerly wind anomalies to its south side over the TWCP. This is verified by a scatter plot of the March AL-related westerly wind anomalies over the TWCP against the March AL-related SLP anomalies over the subtropical western-central North Pacific (Fig. 4b). In decades when the March AL-generated cyclonic anomaly over the subtropical western-central North Pacific is stronger, stronger westerly wind anomalies are induced over the TWCP (Fig. 4b). This further contributes to a stronger influence of the March AL on the following winter ENSO (Fig. 4c).

The interaction between the synoptic-scale eddy activity and low frequency mean flow plays an important role in the formation of the March AL-related cyclonic anomaly over the subtropical North Pacific³⁰. A stronger cyclonic anomaly implies a stronger synoptic-scale eddy activity feedback to the mean flow. This is confirmed by a comparison of the geopotential height tendency anomalies related to the early-spring ALI before and after the late-1990s (Fig. 3c, d). Particularly, negative geopotential height tendency anomalies over the subtropical North Pacific are more prominent and extend more southward during 1996–2020

(Fig. 3c) compared to those before the late-1990s (Fig. 3d), suggesting an enhanced high-frequency transient eddy vorticity feedback to the mean flow and explaining enhancement of the Mar(0) ALI-generated cyclonic anomalies over subtropical North Pacific after the late-1990s. Strength of the synoptic-scale eddy activity feedback to mean flow is impacted by the zonal wind anomalies induced by the AL and the mean state of the background zonal wind over the mid-latitude North Pacific^{35–39}. Stronger zonal wind anomalies can lead to strengthened feedback of the synoptic-scale eddy to low frequency flow if background mean flow is the same^{37–39}. Similarly, if the amplitude of the zonal wind perturbation is the same, strength of the synoptic-scale eddy feedback to mean flow is closely associated with the intensity of the background zonal wind^{37–39}.

A scatter plot of the March AL-related SLP anomalies averaged over the subtropical western-central North Pacific against the AL-related SLP anomalies averaged over the mid-latitude North Pacific shows that the change in the strength of the March AL-related atmospheric anomaly over subtropical North Pacific is not due to change in the amplitude of the AL (Supplementary Figs. 5–6). It implies that the change in the background zonal wind should be a factor for the difference in the AL-related cyclonic anomaly over the subtropical North Pacific. To confirm this, we construct a scatter plot of the March AL-related SLP anomalies over the subtropical western-central North Pacific against the strength of the climatological 500-hPa zonal wind averaged over

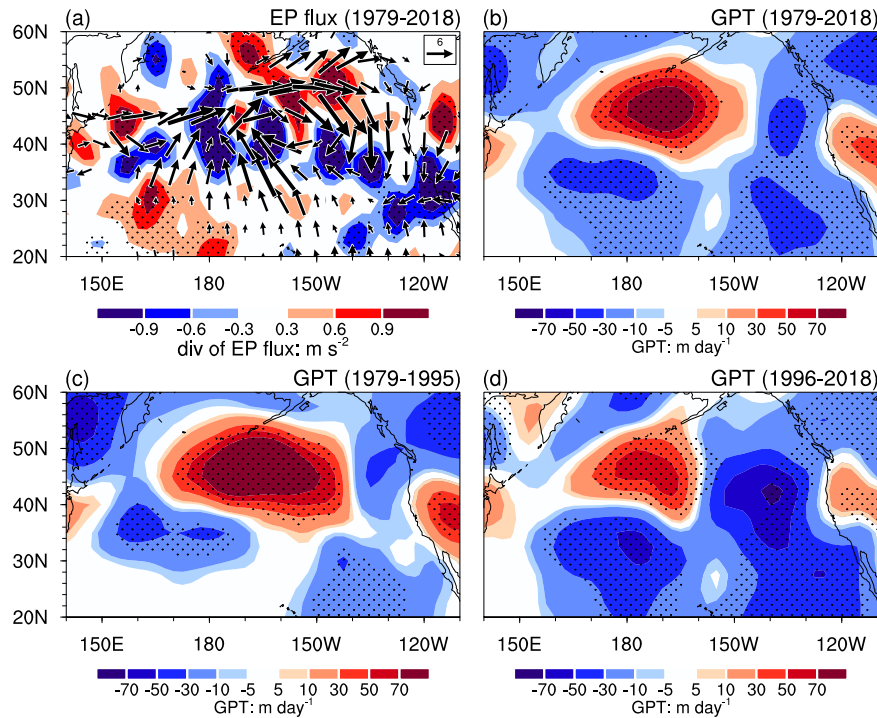


Fig. 3 Interaction between synoptic-scale eddy and low frequency flow over North Pacific associated with the early-spring ALI. Anomalies of **a** extended EP flux (vectors, $\text{m}^2 \text{s}^{-2}$) and divergence of the extended EP flux (shadings, $\text{m}^2 \text{s}^{-2}$), and **b** geopotential height tendency ($\text{m} \text{day}^{-1}$) at 300 hPa in Mar(0) regressed onto the normalized ALI in Mar(0) over 1979–2018. **c–d** as in **b**, but over 1979–1995 and 1996–2018, respectively. Stippling region in **a** indicates EP flux divergence anomalies significant at the 95% confidence level. Stippling regions in **b–d** indicate geopotential height tendency anomalies significant at the 95% confidence level.

the mid-latitude North Pacific in Fig. 4d. Overall, when the mid-latitude background zonal wind is stronger, the easterly wind anomalies over the mid-latitude North Pacific lead to a stronger cyclonic anomaly over the subtropical North Pacific (Fig. 4d) via wave-mean flow interaction^{30,35–39}, which contributes to stronger westerly wind anomalies over the TWCP (Fig. 4b) and results in a marked impact of the March AL on the winter ENSO (Fig. 4c).

In addition, the air–sea interaction (i.e., the WES feedback) in the subtropical northeastern Pacific also plays a crucial role in maintaining and extending the March AL-related atmospheric and SST anomalies over the subtropics to the deep tropics, which further exert impacts on the occurrence of the following winter ENSO^{31,40,41}. The weakened March AL-generated cyclonic anomaly before the late-1990s cannot induce clear SST warming in the subtropical northeastern Pacific (Supplementary Fig. 4g). This is in sharp contrast to the pronounced warming in the subtropical northeastern Pacific after the late-1990s (Fig. 2g). This implies that the air–sea interaction strength (i.e., WES feedback strength, “Methods”) should be stronger after the late-1990s. The stronger WES feedback over the subtropical northeastern Pacific is favorable to the southwestward propagation of atmospheric variability from the extratropical North Pacific to the tropical central Pacific (Supplementary Fig. 7), and thus exerts impacts on ENSO^{41,42}. Connections of the air–sea coupling strength over the subtropical northeastern Pacific with the March AL-related low-level westerly wind anomalies over the TWCP (Fig. 4e) and with the running correlations between the March ALI and winter Niño3.4 SST index (Fig. 4f) clearly show that when the air–sea coupling is stronger over the subtropical northeastern Pacific, the March AL-generated westerly wind anomalies are stronger over the TWCP (Figs. 2g and 4e), which further contribute to a stronger impact of the AL on the winter ENSO (Fig. 4f).

Mean state of the circulation, especially the climatology of trade wind over subtropical northeastern Pacific, plays a dominant role in determining the strength of the WES feedback

(“Methods”)^{21,40,43}. Particularly, the strength of the WES feedback is determined by the ratio of the background wind perturbation and the mean zonal wind (“Methods”). The stronger mean zonal wind (i.e., easterly) leads to an enhanced upward latent heat flux for the similar wind speed anomalies, corresponding to a stronger air–sea coupling strength and the increased WES feedback efficiency. Therefore, the stronger the subtropical high and the northeasterly trade wind over the subtropical northeastern Pacific results in a larger air–sea coupling strength, which contributes to stronger March AL-related westerly wind anomalies over the TWCP, and thus leads to an increased impact on the following winter ENSO.

The background spring SLP over the subtropical northeastern Pacific (east of the Hawaiian Islands) is indeed significantly higher after than before the late-1990s, indicating a strengthened subtropical high there (Fig. 5a). Correspondingly, notable easterly wind differences are seen over the subtropical northeastern Pacific, indicating strengthened trade winds (Fig. 5b). The strengthened subtropical high and northeasterly trade winds increase the efficiency of the WES feedback, which contributes to stronger westerly wind anomalies over the TWCP in association with the March AL variation. This assertion is further confirmed by scatter plots of the March AL-related spring 850-hPa zonal wind anomalies over the TWCP against climatological mean spring SLP and spring 850-hPa zonal wind over the subtropical northeastern Pacific in Fig. 5c, d, respectively. The correlation coefficients of the March AL-related westerly wind anomalies averaged over the TWCP with the spring climatological mean SLP and 850-hPa averaged over the subtropical Northeastern Pacific for the 23-year running period are as high as 0.86 and 0.8. Hence, changes in the mean state of the subtropical high and northeasterly trade winds over the subtropical northeastern Pacific are suggested to play an important role in the formation of the TWCP westerly wind anomalies related to the spring AL, via modulating efficiency of the WES feedback. This further determines the strength of the

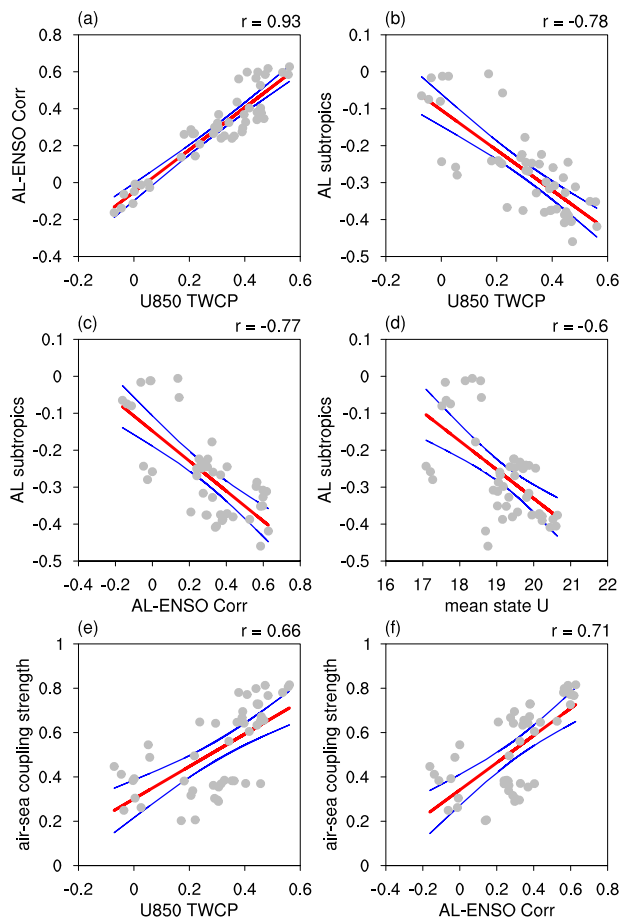


Fig. 4 Factors contribute to enhanced impact of AL on ENSO. Scatter plots of the Mar(0) ALI-related 850-hPa winds anomalies in AM(0) averaged over tropical western-central Pacific (TWCP, box in Fig. 2b) for 23-year running period against **a** the 23-year running correlations between the Mar(0) ALI and D(0)JF(+1) Niño-3.4 SST index, and against **b** the Mar(0) SLP anomalies averaged over subtropical North Pacific (box in Fig. 2a). Scatter plots of the Mar(0) SLP anomalies averaged over subtropical North Pacific against **c** the 23-year running correlations of the Mar(0) ALI and D(0)JF(+1) Niño-3.4 SST index, and against **d** the climatology of 500-hPa zonal wind averaged over mid-latitude North Pacific (27.5°N–32.5°N, 135°E–130°W). Scatter plots of the air-sea coupling strength over the subtropical northeastern Pacific (see “Methods”) against **e** the 850-hPa zonal wind anomalies averaged over the TWCP, and against **f** the 23-year running correlations between the Mar(0) ALI and D(0)JF(+1) Niño-3.4 SST index. Red lines indicates the best linear fit. Blue lines indicate the 95% confidence range of the linear regression.

impact of the March AL on the following winter ENSO. It is noted that the strengthened subtropical high around the late-1990s could have also contributed to the strengthened climatology westerly wind over the mid-latitude North Pacific, which leads to increased wave-mean flow interaction and results in stronger AL-related cyclonic anomaly over the subtropical North Pacific as discussed above.

Factors leading to the strengthened trade winds after the late-1990s

Above analysis indicates that the strengthened air-sea coupling over the subtropical northeastern Pacific due to the strengthened trade winds is crucial for the increased impact of the March AL on the following winter ENSO after the late-1990s. The late-1990s is also the time that the Atlantic Multidecadal Oscillation (AMO)

shifts from its negative to positive phase^{44,45} (Fig. 6a). Spring SLP and easterly winds over the subtropical northeastern Pacific are significantly stronger during a positive AMO phase compared to a negative AMO phase (Fig. 6c, e). Thus, the AMO phase shift may lead to strengthened subtropical high and background trade winds over the subtropical Northeastern Pacific, which can result in increased efficiency of the WES feedback, favorable for strong impacts of the March AL on the winter ENSO after the late-1990s.

We have further examined the impacts of AMO on the subtropical high and trade winds over the subtropical North Pacific via North Atlantic pacemaker experiments conducted by version 6 of the Institute Pierre Simon Laplace model (IPSL-CM6A-LR) that participated in CMIP6 Decadal Climate Prediction Project (DCPP) (see “Pacemaker experiments” in “Methods”). For the North Atlantic pacemaker experiments (NATL-PMExp), the model was forced by time-varying historical radiative forcings based on CMIP6 protocol, but SST was restored to the observed historical SST variation in the North Atlantic. In other regions, the model is free coupled. The NATL-PMExp covers the period from 1920 to 2014, and consists of ten realizations in which the integrations begin from different initial conditions. The NATL-PMExp can well reproduce phase evolution of AMO index (Fig. 7a; see “Methods” for the definition of AMO). We used ensemble mean of the ten realizations of NATL-PMExp to examine the impacts of AMO. Similar to the observations, subtropical high and background trade winds over subtropical Northeastern Pacific are stronger during positive than negative AMO phases in the NATL-PMExp (Fig. 7b, c). The NATL-PMExp also shows strengthened zonal wind over the mid-latitude North Pacific, which contribute to increased wave-mean flow interaction and stronger AL-related cyclonic anomaly over the subtropical North Pacific as discussed above. Thus, the NATL-PMExp further suggests that the AMO may play an important role in the enhanced impact of the March ALI on the following winter ENSO after the late-1990s via enhancement of North Pacific mean circulation and associated enhanced wave-mean flow interaction and air-sea coupling.

In addition to the AMO, Pacific Decadal Oscillation (PDO) and North Pacific Gyre Oscillation (NPGO) are also important interdecadal climate variability modes over the North Pacific. PDO index is in its positive phase around the late 1990s (Supplementary Fig. 8a). It indicates that change in the PDO phase occurred at a time different from the change in the connection of March AL with the ENSO. Further, SLP and zonal wind anomalies over the subtropical northeastern Pacific are weak around 10°–20°N between positive and negative PDO phases (Supplementary Fig. 8b, c). This suggests that the phase change of the PDO does not likely contribute to enhanced trade winds and the associated increased air-sea coupling after the late-1990s. By contrast, a positive NPGO phase contributes to stronger spring SLP and easterly winds over the subtropical northeastern Pacific (Fig. 6d, f). This implies that the change of the NPGO from its negative to positive phases around the late-1990s may also has a considerable contribution to the increased air-sea coupling and the strengthened spring AL-ENSO connection via enhancing the subtropical high and trade winds. In addition, the NPGO is in its negative phase before the early-1960s, which contributes to weakened subtropical high and trade winds over the subtropical northeastern Pacific. The possible interference of the negative NPGO phase may be a reason why the previous positive phase of the AMO (during 1930s–1960s) was not accompanied by enhanced spring AL-winter ENSO connection.

Recent studies indicated that the global warming would enhance the air-sea coupling strength over the subtropical North Pacific and lead to strengthened impact of the PMM on winter ENSO occurrence^{46–48}. Further, studies indicated that occurrence of the CP ENSO events⁴⁹ and winter AL intensity will increase under greenhouse warming⁵⁰. This suggests that the enhanced impact of the early-spring AL on the following winter ENSO during

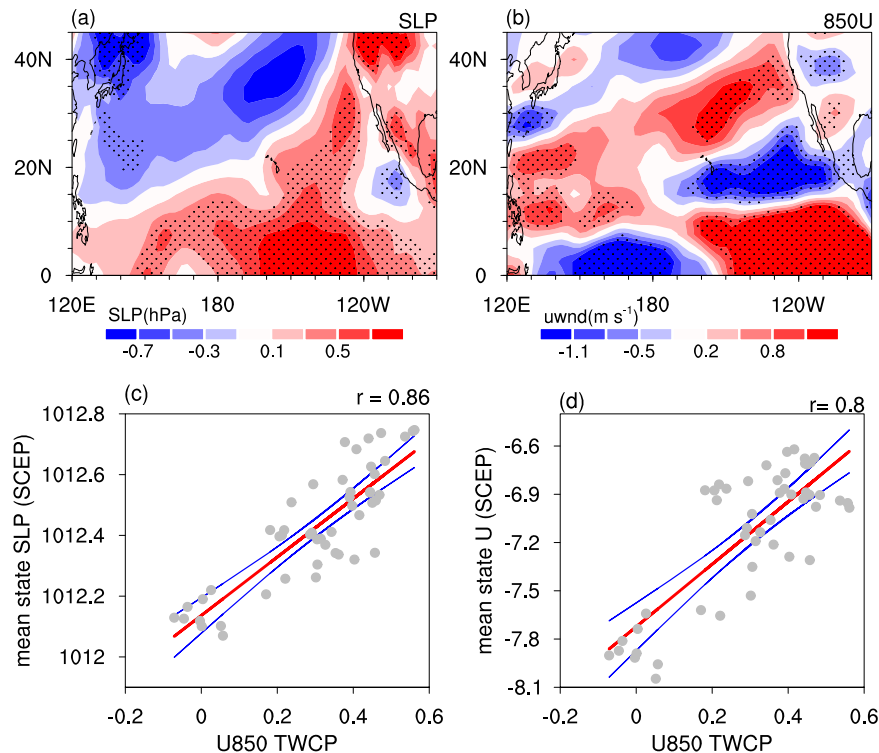


Fig. 5 Pacific mean states change. Differences in the climatology of spring **a** SLP and **b** 850-hPa zonal wind between periods 1996–2018 and 1949–1995. Stippling regions in **a**, **b** indicate the differences that are significantly different from zero at the 95% confidence level. Scatter plots of the Mar(0) ALI-related 850-hPa zonal wind anomalies in AM(0) averaged over the TWCP against the climatology of spring **c** SLP and **d** 850-hPa zonal wind over the subtropical northeastern Pacific for the 23-year running period. Red lines indicate the best linear fit. Blue lines indicate the 95% confidence range of the linear regression.

recent decades may be due to the global warming. We have preliminarily examined whether global warming has a contribution to the enhancement of the background mean easterly winds over the subtropical North Pacific. We calculated the differences in mean spring 850-hPa zonal wind between historical simulations over 1920–1999 and SSP-585 simulations over 2020–2099 from 34 CMIP6 models (Supplementary Table 2). All the individual CMIP6 models, as well as their ensemble mean, project weakened trade winds over the subtropical Northeastern Pacific under the global warming (Fig. 8). To exclude the possible impact of the internal climate variability, we have also used the 50-member large ensemble simulations conducted with the CanESM2 (“Methods”). Differences in mean spring 850-hPa zonal wind over periods 2045–2100 (following RCP85 scenario) and 1950–2005 (historical simulation) in the 50 individual members and their ensemble mean confirm a weakened springtime trade wind over the subtropical northeastern Pacific under global warming (Supplementary Fig. 9). Above evidences indicate that global warming tends to lead to decrease in climatological mean trade winds. This implies that the enhanced trade wind over subtropical North Pacific after the late-1990s may not be related to greenhouse warming. Nevertheless, it is still unclear whether global warming could exert impact on the March AL-ENSO connection via other mechanisms. The relative roles of the internal climate variability and global warming in contributing to the recent enhanced impact of the early spring AL on the following winter ENSO around the late-1990s should be further investigated.

Subtropical wind stress curl anomalies induced by the early-spring AL may be able to lead to a charge or discharge of the subsurface ocean heat content in the tropical central Pacific^{21–23}. Particularly, decrease in the intensity of AL in March lead to cyclonic anomalies and southwesterly wind anomalies over the subtropical North Pacific. This could provide negative surface wind

stress curl anomalies to its south over the tropical North Pacific. These negative wind stress curl anomalies lead to downward Ekman Pumping and meridional Sverdrup transport toward the tropical central Pacific^{21–23}, which would increase the subsurface temperature over the tropical Pacific that is conducive to the El Niño onset. We compare this mechanism by regressing MAM(0) surface wind stress curl anomalies over the tropical North Pacific onto the normalized Mar(0) ALI over 1979–1995 and 1996–2018. It shows that weakened ALI could induce negative surface wind curl anomalies over tropical North Pacific during both 1979–1995 and 1996–2018 (Supplementary Fig. 10a, b). However, the negative surface wind curl anomalies during 1996–2018 are much weaker and located more northward compared to those before the late-1990s (Supplementary Fig. 10c). This implies that enhanced impact of the early-spring ALI on the following winter ENSO is not likely attributed to change in the trade wind charging mechanism.

DISCUSSION

This study reveals a pronounced enhanced impact of the March AL on the subsequent winter ENSO after the late-1990s, which may play a critical role for the increased occurrence of CP ENSO events during recent decades. The change in the March AL-winter ENSO connection is found to be related to the change in the mean state of atmospheric circulation over the North Pacific. The stronger mean zonal wind over the mid-latitude North Pacific after the late-1990s leads to increased wave-mean flow interaction, and results in strengthened cyclonic anomaly over the subtropical North Pacific and westerly wind anomalies over the TWCP. This contributes to a stronger impact of the March AL on the following winter ENSO. In addition, stronger mean trade winds after the late-1990s lead to increased air-sea coupling and WES feedback over

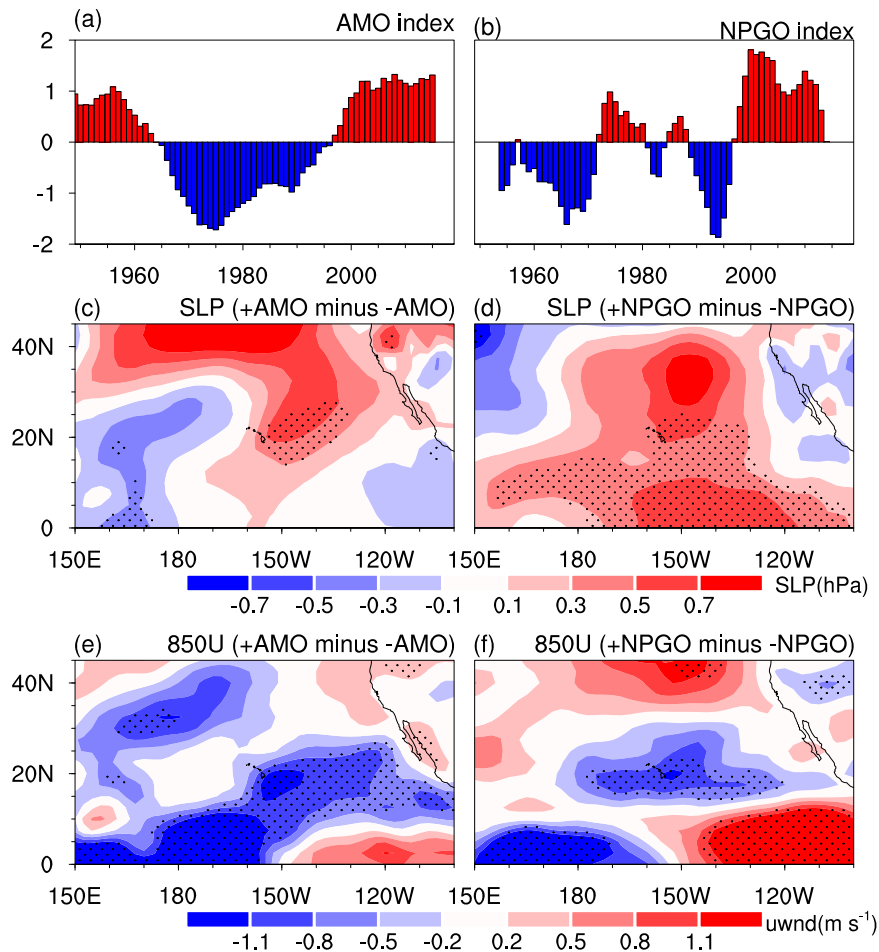


Fig. 6 Modulations of the AMO and NPGO on the Pacific mean states in the observations. Normalized time series of the annual mean **a** AMO index and **b** NPGO index with 9-year running mean. Differences in the climatology of spring SLP **c** between positive and negative AMO phases, and **d** between positive and negative NPGO phases. **e**, **f** as in **c**, **d**, but for differences in the climatology of spring 850-hPa zonal wind between different phases of the AMO and NPGO. Stippling regions in **c**–**f** indicate the differences that are significantly different from zero at the 95% confidence level.

the subtropical northeastern Pacific. Thus, the March AL-generated cyclonic anomaly and ocean surface warming in the subtropics can easily penetrate to the deep tropics and impact the following winter ENSO. Our analysis also indicates that changes of both the AMO and NPGO from positive to negative phases around the late-1990s contribute to the enhancement of the mean trade wind and WES feedback over the subtropical northeastern Pacific.

This study indicates the early-spring AL has an impact on ENSO. It is noted that AL tends to peak in boreal winter (Supplementary Fig. 11). Variability of the AL intensity in boreal winter is also larger than that in early-spring (Supplementary Fig. 12). Standard deviation of the March ALI is about 74% of that in boreal winter. A question is whether AL variabilities in boreal winter and other months also have an impact on the following ENSO. To address this issue, we have examined running correlations of the monthly ALI from November to April with the following winter Niño-3.4 SST index (Supplementary Fig. 13). It shows that, besides March ALI, ALI in other months has a weak relationship with the D(0)JF(+1) Niño-3.4 SST index over the whole analysis period (Supplementary Fig. 13a–f). It is still unclear why only March ALI has a significant effect on the following ENSO, which deserves further study. Notice that the similar results are obtained based on the ALI in FMA (i.e. February–March–April–average), MA (March–April–average) or MAM (March–April–May–average), but with a slight weaker amplitude of the signals (Supplementary Fig. 13g–j).

ENSO has a strong asymmetric feature in its amplitude and climatic impacts⁵¹. A natural question is whether the impact of the early-spring ALI on the following winter ENSO is asymmetry or not. In section 2, we have shown that 7 out of 8 weakened March AL years are followed by El Niño events in the subsequent winter after the late-1990s (Supplementary Table 1). In addition, 6 out of the 7 enhanced March AL years are followed by La Niña events (Supplementary Table 1). Thus, the occurrence ratio of weakened AL years preceding El Niño (87.5%) is comparable to that of strengthened AL years followed by La Niña (85.7%). This suggests that the impacts of March ALI on both El Niño and La Niña are evident after the late-1990s. We have further examined evolutions of SST anomalies related to the weakened and strengthened ALI years (Supplementary Fig. 14). It shows that decrease in the AL intensity in March is followed by a significant El Niño SST warming pattern in the tropical Pacific (Supplementary Fig. 14a–e). Similarly, a La Niña SST cooling pattern is seen when ALI is stronger than normal in preceding March (Supplementary Fig. 14f–j). We note that amplitude of the La Niña cooling (Supplementary Fig. 14j) is much weaker than that of El Niño warming (Supplementary Fig. 14e), suggesting a stronger impact of AL on the El Niño amplitude.

As described above, weakened March AL-generated westerly wind anomalies in the equatorial western Pacific (Fig. 2a) can directly impact following winter El Niño via triggering eastward propagating and downwelling equatorial Kelvin and zonal oceanic advection. In addition, the early-spring ALI-induced cyclonic

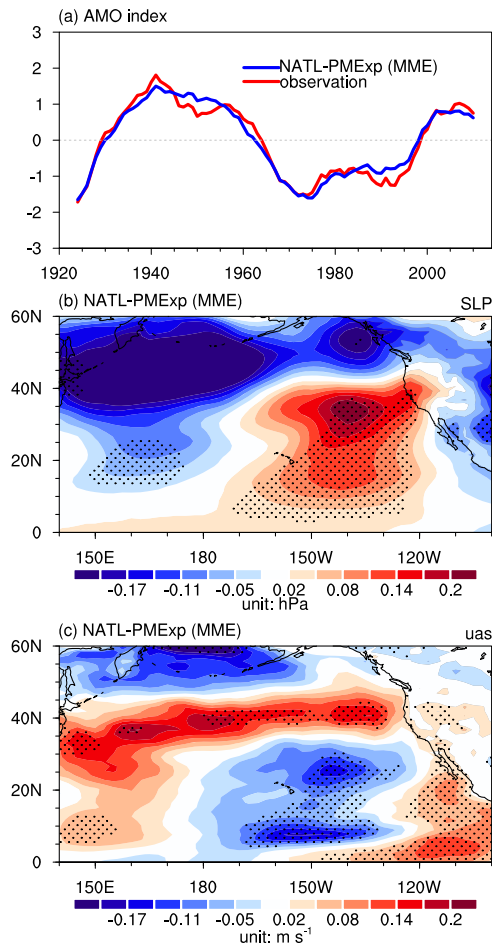


Fig. 7 Modulations of the AMO on the Pacific mean states in the pacemaker experiments. **a** Annual mean AMO index with 9-year running average derived from the observation and ensemble mean of the NATL-PMExp (see “Pacemaker experiments” in “Methods”). Differences of the background mean **b** SLP and **c** surface zonal wind in JFMAM(0) between positive and negative AMO phases in NATL-PMExp. Stippling regions in **b**, **c** indicate the differences that are significantly different from zero at the 95% confidence level.

anomalies could lead to SST warming in following late-spring (Fig. 2g) in the subtropical North Pacific via modulation of surface heat fluxes³⁰. This subtropical North Pacific SST warming could propagate to tropical Pacific, which also play a role in modulating following winter El Niño occurrence. We have further examined the important role of the WES feedback. We first defined a subtropical North Pacific (SNP) SST index as region-mean SST anomalies in AM(0) averaged in SNP (region shown in Fig. 2g). Then, we calculated evolution of SST anomalies regressed upon the Mar(0) ALI after removal of the AM(0) SNP SST index. Mar(0) AL variability still can induce El Niño-like SST warming pattern in the tropical Pacific after removing the effect of the SNP SST anomalies, but with much weaker amplitude and less significant in the tropical Pacific (Supplementary Figs. 15–16). This indicates that WES feedback process also play an important role in relaying the impact of early-spring AL on the following winter ENSO.

Our study indicates that, after the late-1990s, a weaker (stronger) early-spring AL intensity tends to induce an El Niño (La Niña) event in the following winter. Previous studies demonstrated that an El Niño (a La Niña) event tends to lead to a strengthened (weakened) AL^{6,28,29}. Hence, an El Niño event in the first year can be followed by a La Niña event in the second year with the feedback from the strengthened spring AL. Similarly,

a La Niña in the first year can be followed by an El Niño event in the second year with a feedback from the weakened spring AL. This implies that the AL-ENSO interaction may serve as an important phase-transition mechanism during the ENSO cycle with a period of about 2 years, resulting in the quasi-biennial component of the ENSO. Previous studies have demonstrated that the CP type of ENSO shows a significant quasi-biennial component^{45,52}. In addition, the quasi-biennial component of ENSO is suggested to be the major factor responsible for the spring persistence barrier of ENSO⁵². Therefore, the spring AL may to some extent help reduce the spring predictability barrier of ENSO in the current coupled climate models and improve the prediction of ENSO. However, in order to employ the spring AL to forecast ENSO events, the current state of the art coupled climate models should be able to realistically simulate the AL variation as well as the physical process linking the early-spring AL with the following winter ENSO. These issues will be explored in the near future.

The increased occurrence of CP El Niño after the late-1990s has been extensively studied, but the mechanisms of this decadal change in El Niño properties remain under debate⁵³. Several mechanisms have been proposed, including a steeper equatorial thermocline⁵⁴, and a strengthening of eastern Pacific cross-equatorial winds⁵⁵. The strengthened impact of the early spring AL proposed here is an alternative one. It is possible that all the above mechanisms can have contributions in the observations.

METHODS

Observations and reanalysis data

We use the monthly mean SLP, winds at 850-hPa and 500-hPa, precipitation rate, surface heat fluxes (including surface latent and sensible heat fluxes, net surface shortwave and longwave radiations) provided by the National Centers for Environmental Prediction-National Center for Atmospheric Research reanalysis dataset from January 1948 to the present (NCEP-NCAR)⁵⁶. Values of the surface heat fluxes were taken to be positive (negative) when their directions are downward (upward), which contribute to surface warming (cooling). We also employ the daily mean geopotential height and winds from the NCEP-NCAR reanalysis to calculate synoptic-scale eddy activity (also called storm track). Monthly mean SST provided by the National Oceanic and Atmospheric Administration (NOAA) Extended Reconstructed SST version 5 from January 1854 to the present⁵⁷. Monthly mean precipitation data from January 1979 to the present are obtained from the Climate Prediction Center Merged Analysis of Precipitation (CMAP) dataset⁵⁸. In addition, monthly mean surface wind stress, mixed layer depth, zonal current, meridional current, vertical current, and subsurface sea water potential temperature are extracted from the Global Ocean Data Assimilation System reanalysis dataset from January 1980 to the present⁵⁹. The variables from the GOADS all have a zonal resolution of 1° and meridional resolution of 1/3°.

CMIP6 data

To examine the effect of global warming on the background circulation, we compare the historical simulations and the climate change projection simulations under the SSP585 scenario from 34 coupled climate models that participated in CMIP6⁶⁰ (Supplementary Table 2). As a number of models only provide one member in the historical simulation or the climate change simulation, we only employ the first run from these 34 CMIP6 models. Mean state differences of interested variables between SSP585 scenario (2020–2099) and historical (1920–1999) simulations from the 34 CMIP6 models are used to represent the influence of the global warming. We use the 80-year mean to reduce the impact of internal climate variability as much as possible.

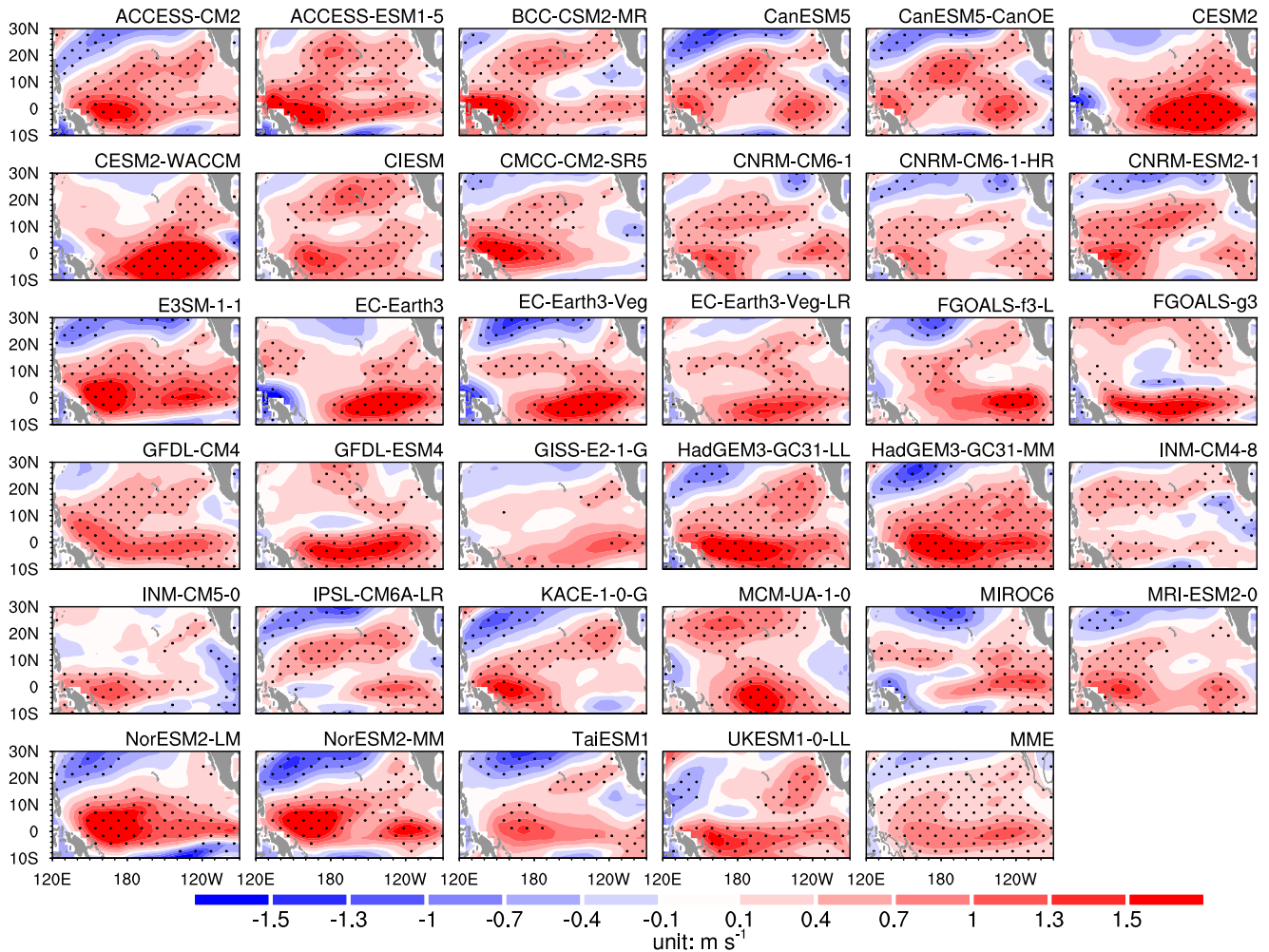


Fig. 8 Change in the mean state of low-level zonal wind under global warming in CMIP6. Differences in the background mean spring 850-hPa zonal wind between present-day climate period (historical simulations over 1920–1999) and future climate period (SSP-585 simulations over 2020–2099) for 34 CMIP6 models (Supplementary Table 2) and their MME. Stippling regions indicate the differences that are significantly different from zero at the 95% confidence level.

Large ensemble experiments of CanESM2

We use the 50-member large ensemble climate simulations conducted with the second-generation Canadian Earth System Model to further confirm the effect of the global warming on the mean climate, which largely exclude the contribution of the internal climate variability (CanESM2)^{61,62}. The 50-member climate simulations of CanESM2 are briefly summarized as follows. First, five simulations are constructed over 1850–1950 to develop five different oceanic conditions in 1950. Second, ten simulations are further performed from each of the above five simulations with small different initial conditions in 1950. Due to the chaotic nature of climate systems, the small different initial condition in 1950 results in quite different atmospheric states a few days later. This produces 50 members of simulations over the period 1950–2100. Over 1950–2005, each of the simulations is forced with the same historical radiative forcings, sulfate aerosols, and greenhouse gas concentration. Over 2006–2100, the simulations are forced by the RCP8.5 scenario forcing⁶³. We compare the mean state differences between 2045–2100 and 1950–2005 in the CanESM2 simulations. Because each of the simulations is forced by the same external forcing with only slight differences in the initial condition, the difference of the projected changes among the 50 members is due solely to internal climate variability. In addition, projected changes due to the external forcing can be obtained by averaging the results of the CanESM2 50 members.

Synoptic scale eddy activity

Synoptic scale eddy activity (also called storm track) is calculated as the root mean square of the 2–8 day band-pass filtered geopotential height anomalies at a given pressure level⁶⁴.

Extended EP flux

The Extended Eliassen-Palm (EP) flux^{35,65} was employed to qualitatively evaluate the dynamical interaction between synoptic-scale eddy activity and low frequency mean flow, which is expressed as follows:

$$E_u = \left[\frac{1}{2} (\overline{v'^2} - \overline{u'^2}) \vec{i}, -\overline{u'v'} \vec{j} \right] \times \cos \phi \quad (1)$$

where u' , and v' indicate synoptic-scale zonal and meridional winds, respectively, obtained by applying a band-pass filter to the raw daily fields to isolate variation on the 2–8-day timescale. ϕ denotes the latitude. The overbar represents the monthly mean.

Geopotential height tendency

Feedback of the synoptic-scale eddy activity to low frequency mean low can be quantitatively estimated by the feedback term in the geopotential height tendency equation^{35,36}. The geopotential height tendency due to the eddy vorticity flux forcing is expressed

as follows:

$$F = \frac{f}{g} \nabla^{-2} \left[-\nabla \cdot (\overline{\mathbf{V}'\zeta'}) \right] \quad (2)$$

Here f and g denote the Coriolis parameter and the acceleration of gravity, respectively. ζ' and \mathbf{V}' represent the synoptic-scale vorticity and winds, respectively.

Mixed layer height budget

To examine the processes for the formation of SST anomalies in the tropical Pacific induced by the Mar(0) ALI, we diagnose the mixed layer heat budget^{66,67}. The mixed layer heat budget equation is written as follows:

$$\underbrace{\frac{\partial T_a}{\partial t}}_{\text{Tendency}} = - \underbrace{\left(u_a \frac{\partial T_a}{\partial x} + v_a \frac{\partial T_a}{\partial y} \right)}_{\text{Horizontal advection}} + \underbrace{k_H \left(\frac{\partial^2 T_a}{\partial x^2} + \frac{\partial^2 T_a}{\partial y^2} \right)}_{\text{Horizontal mixing}} - \underbrace{\frac{1}{h} \left[k_z \frac{\partial T_a}{\partial z} \right]_{-h}}_{\text{Vertical mixing}} - \underbrace{\left(\frac{T_a - T_{-h}}{h} \right) \left(\frac{\partial h}{\partial t} + w_{-h} + u_{-h} \frac{\partial h}{\partial x} + v_{-h} \frac{\partial h}{\partial y} \right)}_{\text{Entrainment}} + \underbrace{\frac{q_0 - q_{\text{pen}}}{\rho_0 C_p h}}_{\text{Net heat flux}} \quad (3)$$

where, u_a , v_a and T_a denote the zonal and meridional current velocities and oceanic temperature averaged in the mixed layer depth (h), respectively. h is the temporally and spatially varying mixed layer depth. T_{-h} , u_{-h} , v_{-h} and w_{-h} are the oceanic temperature, zonal, meridional, and vertical velocity at the base of the mixed layer, respectively. C_p denotes the ocean heat capacity, ρ_0 is sea water density, q_{pen} is the penetrative loss of shortwave radiation, and q_0 denotes the surface net heat flux. q_0 is the sum of the surface net shortwave radiation, surface net longwave radiation, surface sensible heat flux and the surface latent heat flux. k_z and k_H denote the vertical and horizontal eddy diffusivities, respectively.

The terms of horizontal mixing ($k_H \left(\frac{\partial^2 T_a}{\partial x^2} + \frac{\partial^2 T_a}{\partial y^2} \right)$), vertical mixing ($\frac{1}{h} \left[k_z \frac{\partial T_a}{\partial z} \right]_{-h}$), and penetrating shortwave radiation (q_{pen}) are much smaller compared to other terms^{66,67}. Therefore, the terms of horizontal mixing, vertical mixing and penetrating shortwave radiation could be omitted. Thus, the above mixed layer heat budget equation can be further simplified as follows:

$$\frac{\partial T_a}{\partial t} = -u_a \frac{\partial T_a}{\partial x} - v_a \frac{\partial T_a}{\partial y} - w_e \frac{T_a - T_{-h}}{h} + \frac{q_0}{\rho_0 C_p h} + R \quad (4)$$

$$w_e = \frac{\partial h}{\partial t} + w_{-h} + u_{-h} \frac{\partial h}{\partial x} + v_{-h} \frac{\partial h}{\partial y} \quad (5)$$

In Eq. (4), $\frac{\partial T_a}{\partial t}$ is oceanic temperature tendency term; $-u_a \frac{\partial T_a}{\partial x} - v_a \frac{\partial T_a}{\partial y}$ represent horizontal advection term; $-w_e \frac{T_a - T_{-h}}{h}$ is entrainment term; $\frac{q_0}{\rho_0 C_p h}$ represent net heat flux term. R denotes the residual term which represents unresolved processes, including vertical and lateral diffusion and high frequency eddies. w_e is calculated via Eq. (5), including vertical advection (w_{-h}), lateral induction ($u_{-h} \frac{\partial h}{\partial x} + v_{-h} \frac{\partial h}{\partial y}$) and mix layer tendency ($\frac{\partial h}{\partial t}$).

Pacemaker experiments

We examined the impact of AMO on the Pacific mean states via North Pacific Pacemaker experiments (denoted as NATL-PMExp) conducted by version 6 of the Institut Pierre Simon Laplace model (IPSL-CM6A-LR) that participated in CMIP6 Decadal Climate Prediction Project (DCPP)⁶⁸. In the NATL-PMExp, the model was forced by time-varying historical radiative forcings based on CMIP6 simulation protocol, with the SST was restored to the observed historical SST variation in the North Atlantic. In other

regions, the model is free coupled. The detailed design of the Pacemaker experiments is referred to⁶⁹. The NATL-PMExp cover the period from 1920 to 2014, and consist of ten realizations that the integrations begin with different initial conditions. We used ensemble mean of the ten realizations of NATL-PMExp to examine the impacts of AMO.

PMM and air-sea coupling strength

Studies have indicated that the PMM is the first leading air-sea coupling mode over the subtropical Northeastern Pacific^{31,32,41}. The PMM is defined as the first singular value decomposition (SVD, also called maximum covariance analysis, MCA) mode of the SST and surface winds anomalies over the subtropical Northeastern Pacific^{31,32,41}. As in previous studies, strength of the air-sea coupling (i.e., WES feedback) over the subtropical northeastern Pacific is defined as the correlation coefficient between the PMM-SST and PMM-wind indices^{41,42,70}. The PMM-SST (PMM-wind) index is represented by expansion coefficient time series of SST (surface winds) corresponding to the first SVD of SST and surface winds over the subtropical Northeastern Pacific.

Efficiency of the WES feedback

Following previous studies^{21,40,43}, the efficiency of the WES feedback (α , representing change in the surface latent heat flux per unit anomalies of the surface wind) is expressed as follows:

$$\alpha = -\frac{\partial \text{LH}}{\partial u} \approx -\frac{u}{\sqrt{u^2 + w'^2}} = -\frac{1}{\sqrt{1 + \left(\frac{w'}{u}\right)^2}} \quad (6)$$

Here w' represents the background wind speed perturbation, u is the background mean zonal wind. It should be mentioned that the zonal wind component dominates the change in the WES feedback, and thus the contribution of the meridional wind is not considered^{21,40,43}.

AL and NPO

We use EOF analysis to obtain the AL and NPO variation patterns. The first two leading EOF modes of March SLP anomalies over North Pacific (20°–70°N, 120°E–100°W) during 1979–2019 are shown in Supplementary Fig. 1. EOF1 is characterized by same-sign SLP anomalies over mid-high latitudes of the North Pacific, with the largest loading around the region where the climatological Aleutian Low generally is located. Thus, EOF1 represents variation of the Aleutian Low intensity (ALI). According to the spatial pattern shown in Supplementary Fig. 1a, we define an ALI as region-mean SLP anomalies over the area of 30°–65°N, 160°E–140°W. Note that positive value of ALI corresponds to a weakened AL intensity. The correlation coefficient between the ALI and the principal component (PC) time series of EOF1 is as high as 0.95 over 1979–2019. EOF2 of the SLP anomalies over the North Pacific is featured by a meridional dipole pattern, which represents the NPO (Supplementary Fig. 1b). The NPO index is defined as the PC time series corresponding to the EOF2 of SLP anomalies.

AMO

The Atlantic Multidecadal Oscillation (AMO) is the dominant SST variability on the multidecadal time scale in the North Atlantic⁴⁴. Monthly mean smoothed AMO index since the January 1948 is obtained from the NOAA Physical Science Division (Fig. 6a). A positive (negative) AMO phase is defined as those years when the normalized AMO index is larger (smaller) than zero. In the NATL-PMExp, the AMO index is defined as detrended SST anomalies averaged in North Atlantic (0°–70°N and 0°–60°W)⁷¹.

PDO

The Pacific Decadal Oscillation (PDO) is the first leading mode of SST variability on the decadal time scale over the North Pacific⁷². Monthly mean PDO index is extracted from the NOAA Physical Sciences Laboratory available from January 1948 to the present (Supplementary Fig. 8a). A positive (negative) PDO phase is defined as those years when the normalized PDO index is larger (smaller) than zero.

NPGO

The North Pacific Gyre Oscillation (NPGO) is the second EOF mode of sea surface height variation over the North Pacific, and it is characterized by interdecadal changes in the oceanic gyres over the subtropical and subpolar North Pacific⁷³. Monthly mean North Pacific Gyre Oscillation (NPGO) index is derived from <http://www.o3d.org/npgo/>, covering the period from January 1950 to the present (Fig. 6b). A positive (negative) NPGO phase is defined as those years when the normalized NPGO index is larger (smaller) than zero.

ENSO variability

ENSO variability is characterized by the Niño-3.4 SST index, which is defined as region-mean SST anomalies over 5°S–5°N, 120°–170°W. As ENSO has a strong quasi-biennial oscillation feature and has a strong impact on the AL, we remove preceding winter (December–March–mean, DJFM) Niño-3.4 SST index influence from the March AL index and all other variables based on a linear regression. This ensures that the connection of the March AL with the following winter ENSO is independent of the influence of preceding ENSO.

Statistical significance

Long-term linear trend and climatological seasonal cycle of all variables have been removed. Significance levels of regression and correlation coefficients are estimated by a two-tailed Student's *t* test.

Effective degree of freedom

Considering the auto-correlation of the time series, the effective degree of freedom (N^*) is estimated as follows⁷⁴:

$$N^* = N \times \frac{1 - r_1 \times r_2}{1 + r_1 \times r_2} \quad (7)$$

where N is the raw length of the time series. r_1 and r_2 are the lag one auto-correlation coefficients of the two time series used to calculate the correlation.

Fisher's *r-z* transformation

Fisher's *r-z* transformation is used to estimate significance level of the difference between two correlation coefficients (denoted as R_1 and R_2). The Fisher transform of R_1 and R_2 can be written as follows⁷⁵:

$$Z_1 = \frac{1}{2} \ln \left[\frac{1 + R_1}{1 - R_1} \right], \quad (8)$$

$$Z_2 = \frac{1}{2} \ln \left[\frac{1 + R_2}{1 - R_2} \right]. \quad (9)$$

Then, the standard parametric test is employed to estimate the null hypothesis of the equality of the Z_1 and Z_2 . The test statistic u

is written as:

$$u = \frac{Z_1 - Z_2}{\sqrt{\frac{1}{N_1 - 3} + \frac{1}{N_2 - 3}}}, \quad (10)$$

Here, N_1 and N_2 are the sizes of the data used to calculate R_1 and R_2 , respectively. The test statistic u is normal distribution. Hence, the significance levels are evaluated based on the two-tailed Student's *t* test.

DATA AVAILABILITY

The NCEP-NCAR reanalysis data are obtained from <https://psl.noaa.gov/data/gridded/data.ncep.reanalysis.html>. The SST data are derived from <https://psl.noaa.gov/data/gridded/data.noaa.erst.v5.html>. The GODAS data are extracted from <https://www.cpc.ncep.noaa.gov/products/GODAS/>. The AMO index is obtained from <https://www.esrl.noaa.gov/psd/data/timeseries/AMO/>. The PDO index is extracted from <https://psl.noaa.gov/data/correlation/pdo.data>. The NPGO index is derived from <http://www.o3d.org/npgo/>. CMAP precipitation data are obtained from <https://www.psl.noaa.gov/data/gridded/data.cmap.html>. The CMIP6 data and the pacemaker experiments data are derived from <https://esgf-node.llnl.gov/projects/cmip6/>. The CanESM2 data are obtained from <https://open.canada.ca/en>.

CODE AVAILABILITY

The code associated with this manuscript is available on request from the corresponding author.

Received: 4 November 2022; Accepted: 9 March 2023;

Published online: 03 April 2023

REFERENCES

- Bjerknes, J. Atmospheric teleconnections from the equatorial Pacific. *Mon. Weather Rev.* **97**, 163–172 (1969).
- Jin, F.-F. Tropical ocean–atmosphere interaction, the Pacific Cold Tongue, and the El Niño–Southern Oscillation. *Science* **274**, 76–78 (1996).
- Neelin, J. D. et al. ENSO theory. *J. Geophys. Res.* **103**, 14261–14290 (1998).
- McPhaden, M. J., Zebiak, S. E. & Glantz, M. H. ENSO as an integrating concept in Earth science. *Science* **314**, 1740–1745 (2006).
- Wang, B., Wu, R. & Fu, X. Pacific–East Asian teleconnection: how does ENSO affect EastAsian climate? *J. Clim.* **13**, 1517–1536 (2000).
- Alexander, M. A. et al. The atmospheric bridge: the influence of ENSO teleconnections on air–sea interaction over the global oceans. *J. Clim.* **15**, 2205–2231 (2002).
- Xie, S.-P. et al. Indian ocean capacitor effect on Indo-Western Pacific climate during the summer following El Niño. *J. Clim.* **22**, 730–747 (2009).
- Zhang, R.-H., Min, Q.-Y. & Su, J.-Z. Impact of El Niño on atmospheric circulations over East Asia and rainfall in China: role of the anomalous western North Pacific anticyclone. *Sci. China Earth Sci.* **60**, 1124–1132 (2017).
- Yeh, S.-W. et al. ENSO atmospheric teleconnections and their response to greenhouse gas forcing. *Rev. Geophys.* **56**, 185–206 (2018).
- Cai, W. et al. Climate impacts of the El Niño–Southern Oscillation on South America. *Nat. Rev. Earth Environ.* **1**, 215–231 (2020).
- Barnston, A. G., Tippett, M. K., L'Heureux, M. L., Li, S. & DeWitt, D. G. Skill of real-time seasonal ENSO model predictions during 2002–11: Is our capability increasing? *Bull. Am. Meteorol. Soc.* **93**, 631–651 (2012).
- Xue, Y., Chen, M. Y., Kumar, A., Hu, Z. & Wang, W. Q. Prediction skill and bias of tropical Pacific sea surface temperatures in the NCEP Climate Forecast System Version 2. *J. Clim.* **26**, 5358–5378 (2013).
- Ashok, K., Behera, S., Rao, A. S., Weng, H. & Yamagata, T. El Niño Modoki and its teleconnection. *J. Geophys. Res.* **112**, C11007 (2007).
- Kao, H.-Y. & Yu, J.-Y. Contrasting eastern Pacific and central Pacific types of ENSO. *J. Clim.* **22**, 615–632 (2009).
- Kug, J.-S., Jin, F.-F. & An, S.-I. Two types of El Niño events: cold tongue El Niño and warm pool El Niño. *J. Clim.* **22**, 1499–1515 (2009).
- Linkin, M. E. & Nigam, S. The north pacific oscillation–west Pacific teleconnection pattern: mature-phase structure and winter impacts. *J. Clim.* **21**, 1979–1997 (2008).
- Anderson, B. T. Tropical Pacific sea-surface temperatures and preceding sea level pressure anomalies in the subtropical North Pacific. *J. Geophys. Res.* **108**, 4732 (2003).

18. Yu, J.-Y. & Kim, S. T. Relationships between extratropical sea level pressure variations and the central Pacific and eastern Pacific types of ENSO. *J. Clim.* **24**, 708–720 (2011).
19. Yu, J.-Y., Lu, M.-M. & Kim, S. T. A change in the relationship between tropical central Pacific SST variability and the extratropical atmosphere around 1990. *Environ. Res. Lett.* **7**, 034025 (2012).
20. Yeh, S.-W., Wang, X., Wang, C. & Dewitte, B. On the relationship between the North Pacific climate variability and the central Pacific El Niño. *J. Clim.* **28**, 663–677 (2015).
21. Amaya, D. J. The Pacific Meridional Mode and ENSO: a review. *Curr. Clim. Chang. Rep.* **5**, 296–307 (2019).
22. Anderson, B. T. & Perez, R. C. ENSO and non-ENSO induced charging and discharging of the equatorial Pacific. *Clim. Dyn.* **45**, 2309–2327 (2015).
23. Chakravorty, S. et al. Testing the Trade Wind Charging mechanism and its influence on ENSO variability. *J. Clim.* **33**, 7391–7411 (2020).
24. Yeh, S.-W., Yi, D. W., Sung, M. K. & Kim, Y. H. An eastward shift of the North Pacific Oscillation after the mid-1990s and its relationship with ENSO. *Geophys. Res. Lett.* **45**, 6654–6660 (2018).
25. Wang, X., Chen, M., Wang, C., Yeh, S.-W. & Tan, W. Evaluation of performance of CMIP5 models in simulating the North Pacific Oscillation and El Niño Modoki. *Clim. Dyn.* **52**, 1383–1394 (2019).
26. Park, J.-H. et al. Role of the climatological intertropical convergence zone in the seasonal footprinting mechanism of the El Niño–Southern Oscillation. *J. Clim.* **34**, 5243–5256 (2021).
27. Wang, S. Y., L'Heureux, M. & Yoon, J. Are greenhouse gases changing ENSO precursors in the Western North Pacific? *J. Clim.* **26**, 6309–6322 (2013).
28. Horel, J. D. & Wallace, J. M. Planetary-scale atmospheric phenomena associated with the Southern Oscillation. *Mon. Weather Rev.* **109**, 813–829 (1981).
29. Straus, D. M. & Shukla, J. Distinguishing between the SST-forced variability and internal variability in mid latitudes: analysis of observations and GCM simulations. *Q. J. R. Meteorol. Soc.* **126**, 2323–2350 (2000).
30. Chen, S.-F., Chen, W., Wu, R., Yu, B. & Graf, H. F. Potential impact of preceding Aleutian Low variation on the El Niño–Southern Oscillation during the following winter. *J. Clim.* **33**, 3061–3077 (2020).
31. Chang, P. et al. Pacific meridional mode and El Niño–Southern Oscillation. *Geophys. Res. Lett.* **34**, L16608 (2007).
32. Chiang, J. C. H. & Vimont, D. J. Analogous Pacific and Atlantic meridional modes of tropical atmosphere–ocean variability. *J. Clim.* **17**, 4143–4158 (2004).
33. Xie, S.-P. & Philander, S. G. H. A coupled ocean–atmosphere model of relevance to the ITCZ in the eastern Pacific. *Tellus* **46A**, 340–350 (1994).
34. Vimont, D. J., Wallace, J. M. & Battisti, D. S. The seasonal footprinting mechanism in the Pacific: implications for ENSO. *J. Clim.* **16**, 2668–2675 (2003).
35. Lau, N.-C. Variability of the observed midlatitude storm tracks in relation to low-frequency changes in the circulation pattern. *J. Atmos. Sci.* **45**, 2718–2743 (1988).
36. Cai, M., Yang, S., van den Dool, H. & Kousky, V. Dynamical implications of the orientation of atmospheric eddies: a local energetics perspective. *Tellus* **59A**, 127–140 (2007).
37. Jin, F.-F. Eddy-induced instability for low-frequency variability. *J. Atmos. Sci.* **67**, 1947–1964 (2010).
38. Jin, F.-F., Pan, L. & Watanabe, M. Dynamics of synoptic eddy and low-frequency flow interaction. Part I: A linear closure. *J. Atmos. Sci.* **63**, 1677–1694 (2006).
39. Chen, S.-F., Yu, B. & Chen, W. An interdecadal change in the influence of the spring Arctic Oscillation on the subsequent ENSO around the early 1970s. *Clim. Dyn.* **44**, 1109–1126 (2015).
40. Vimont, D. J., Alexander, M. & Fontaine, A. Midlatitude excitation of tropical variability in the Pacific: the role of thermodynamic coupling and seasonality. *J. Clim.* **22**, 518–534 (2009).
41. Lin, C. Y., Yu, J.-Y. & Hsu, H.-H. CMIP5 model simulations of the Pacific meridional mode and its connection to the two types of ENSO. *Int. J. Climatol.* **35**, 2352–2358 (2015).
42. Yu, J.-Y. et al. Linking emergence of the central-Pacific El Niño to the Atlantic Multi-decadal Oscillation. *J. Clim.* **28**, 651–662 (2015).
43. Vimont, D. J. Transient growth of thermodynamically coupled variations in the tropics under an equatorially symmetric mean state. *J. Clim.* **23**, 5771–89 (2010).
44. Kerr, R. A. A North Atlantic climate pacemaker for the centuries. *Science* **288**, 1984–1985 (2000).
45. Wang, L., Yu, J.-Y. & Paek, H. Enhanced biennial variability in the Pacific due to Atlantic capacitor effect. *Nat. Commun.* **8**, 14887 (2017).
46. Liguori, G. & Di Lorenzo, E. Meridional modes and increasing Pacific decadal variability under greenhouse forcing. *Geophys. Res. Lett.* **45**, 983–991 (2018).
47. Fan, H. J., Yang, S., Wang, C., Wu, Y. & Zhang, G. Strengthening amplitude and impact of the Pacific Meridional Mode on ENSO in the warming climate depicted by CMIP6 models. *J. Clim.* **35**, 5195–5213 (2022).
48. Jia, F., Cai, W., Lan, B., Wu, L. & Di Lorenzo, E. Enhanced North Pacific impact on El Niño/Southern Oscillation under greenhouse warming. *Nat. Clim. Chang.* **11**, 840–847 (2021).
49. Yeh, S. W. et al. El Niño in a changing climate. *Nature* **461**, 511–514 (2009).
50. Gan, B. et al. On the response of the Aleutian low to greenhouse warming. *J. Clim.* **30**, 3907–3925 (2017).
51. An, S. & Jin, F. F. Nonlinearity and asymmetry of ENSO. *J. Clim.* **17**, 2399–2412 (2004).
52. Yu, J.-Y. Enhancement of ENSO's persistence barrier by biennial variability in a coupled atmosphere–ocean general circulation model. *Geophys. Res. Lett.* **32**, L13707 (2005).
53. Capotondi, A., Wittenberg, A. T., Kug, J. S., Takahashi, K. & McPhaden, M. J. in *El Niño Southern Oscillation in a Changing Climate* (eds McPhaden, M. J., Santoso, A. & Cai, W.) 65–86 (2002).
54. McPhaden, M. J., Lee, T. & McClurg, D. El Niño and its relationship to changing background conditions in the tropical Pacific. *Geophys. Res. Lett.* **38**, L15709 (2011).
55. Hu, S. & Fedorov, A. V. Cross-equatorial winds control El Niño diversity and change. *Nat. Clim. Chang.* **8**, 798–802 (2018).
56. Kalnay, E. et al. The NCEP/NCAR 40-year reanalysis project. *Bull. Am. Meteorol. Soc.* **77**, 437–472 (1996).
57. Huang, B. et al. Extended Reconstructed Sea Surface Temperature version 5 (ERSSTv5), upgrades, validations, and intercomparisons. *J. Clim.* **30**, 8179–8205 (2017).
58. Xie, P. & Arkin, P. A. Global precipitation: a 17-year monthly analysis based on gauge observations, satellite estimates, and numerical model outputs. *Bull. Am. Meteorol. Soc.* **78**, 2539–2558 (1997).
59. Behringer, D. W. & Xue, Y. Evaluation of the global ocean data assimilation system at NCEP: the Pacific Ocean. In *Eighth symposium on integrated observing and assimilation systems for atmosphere, oceans, and land surface* 11–15 (NCEP, 2004).
60. Eyring, V. et al. Overview of the Coupled Model Intercomparison Project Phase 6 (CMIP6) experimental design and organization. *Geosci. Model. Dev.* **9**, 1937–1958 (2016).
61. Rondeau-Genesse, G. & Braun, M. Impact of internal variability on climate change for the upcoming decades: analysis of the CanESM2-LE and CESM-LE large ensembles. *Clim. Chang.* **156**, 299–314 (2019).
62. Yu, B., Li, G., Chen, S.-F. & Lin, H. The role of internal variability in climate change projections of North American surface air temperature and temperature extremes in CanESM2 large ensemble simulations. *Clim. Dyn.* **55**, 869–885 (2020).
63. Vuuren, D. P. et al. The representative concentration pathways: an overview. *Clim. Chang.* **109**, 5–31 (2011).
64. Lee, S. et al. Interdecadal changes in the storm track activity over the North Pacific and North Atlantic. *Clim. Dyn.* **39**, 313–327 (2012).
65. Chen, S., Yu, B. & Chen, W. An analysis on the physical process of the influence of AO on ENSO. *Clim. Dyn.* **42**, 973–989 (2014).
66. Schiller, A. & Ridgway, K. R. Seasonal mixed layer dynamics in an eddy-resolving Ocean circulation model. *J. Geophys. Res.* **118**, 1–19 (2013).
67. Vijith, V., Vinayachandran, P. N. & Webber, B. Closing the sea surface mixed layer temperature budget from in situ observations alone: Operation Advection during BoBBLE. *Sci. Rep.* **10**, 7062 (2020).
68. Boucher, O. et al. Presentation and evaluation of the IPSL-CM6A-LR climate model. *J. Adv. Modeling Earth Sys.* **12**, e2019MS002010 (2020).
69. Kosaka, Y. & Xie, S. P. Recent global-warming hiatus tied to equatorial Pacific surface cooling. *Nature* **501**, 403–407 (2013).
70. Zheng, Y.-Q., Chen, W. & Chen, S.-F. Intermodel spread in the impact of the springtime Pacific Meridional Mode on following-winter ENSO tied to simulation of the ITCZ in CMIP5/CMIP6. *Geophys. Res. Lett.* **48**, e2021GL039345 (2021).
71. Enfield, D. B. et al. The Atlantic multidecadal oscillation and its relation to rainfall and river flows in the continental U.S. *Geophys. Res. Lett.* **28**, 2077–2080 (2001).
72. Mantua, N. J., Hare, S. R., Zhang, Y., Wallace, J. M. & Francis, R. A. Pacific interdecadal climate oscillation with impacts on salmon production. *Bull. Am. Meteorol. Soc.* **78**, 1069–1079 (1997).
73. Di Lorenzo, E. et al. North Pacific Gyre Oscillation links ocean climate and ecosystem change. *Geophys. Res. Lett.* **35**, L08607 (2008).
74. Bretherton, C. S. et al. The effective number of spatial degrees of freedom of a time-varying field. *J. Clim.* **12**, 1990–2009 (1999).
75. Fisher, R. A. On the 'probable error' of a coefficient of correlation deduced from a small sample. *Metron* **1**, 3–32 (1921).

ACKNOWLEDGEMENTS

We thank three anonymous reviewers for their constructive suggestions, which helped to improve the paper. This study was supported jointly by the National Natural Science Foundation of China (Grants 42175039, 42205021 and 42005020) and the Jiangsu Collaborative Innovation Center for Climate Change.

AUTHOR CONTRIBUTIONS

S.C. and W.C. conceived the study, performed the analyses, and wrote the manuscript. B.Y., R.W., H.G., and L.C. contributed to revising the paper and assisted in interpretation of the results.

COMPETING INTERESTS

The authors declare no competing interests.

ADDITIONAL INFORMATION

Supplementary information The online version contains supplementary material available at <https://doi.org/10.1038/s41612-023-00350-1>.

Correspondence and requests for materials should be addressed to Wen Chen.

Reprints and permission information is available at <http://www.nature.com/reprints>

Publisher's note Springer Nature remains neutral with regard to jurisdictional claims in published maps and institutional affiliations.



Open Access This article is licensed under a Creative Commons Attribution 4.0 International License, which permits use, sharing, adaptation, distribution and reproduction in any medium or format, as long as you give appropriate credit to the original author(s) and the source, provide a link to the Creative Commons license, and indicate if changes were made. The images or other third party material in this article are included in the article's Creative Commons license, unless indicated otherwise in a credit line to the material. If material is not included in the article's Creative Commons license and your intended use is not permitted by statutory regulation or exceeds the permitted use, you will need to obtain permission directly from the copyright holder. To view a copy of this license, visit <http://creativecommons.org/licenses/by/4.0/>.

© The Author(s) 2023